Nature. Author manuscript; available in PMC 2015 March 17.

Published in final edited form as:
Nature. 2014 May 22; 509(7501): 512–515. doi:10.1038/nature13205.

Structure of the AcrAB-TolC multidrug efflux pump

Dijun Du[1], **Zhao Wang**[2], **Nathan R. James**[1], **Jarrod E. Voss**[1], **Ewa Klimont**[1], **Thelma Ohene-Agyei**[3], **Henrietta Venter**[4], **Wah Chiu**[2], and **Ben F. Luisi**[1]

[1]Department of Biochemistry, University of Cambridge, Tennis Court Road, Cambridge CB2 1GA, U.K.

[2]National Center for Macromolecular Imaging, Verna and Marrs McLean Department of Biochemistry and Molecular Biology, Baylor College of Medicine, Houston, Texas 77030, U.S.A.

[3]Department of Pharmacology, Tennis Court Road, Cambridge, CB2 1PD, U.K.

[4]School of Pharmacy & Medical Sciences, Sansom Institute for Health Research, University of South Australia, Adelaide SA 5000, Australia

Abstract

The capacity of numerous bacterial species to tolerate antibiotics and other toxic compounds arises in part from the activity of energy-dependent transporters. In Gram-negative bacteria, many of these transporters form multicomponent 'pumps' that span both inner and outer membranes and are driven energetically by a primary or secondary transporter component[1-7]. A model system for such a pump is the acridine resistance complex of *Escherichia coli*[1]. This pump assembly comprises the outer-membrane channel TolC, the secondary transporter AcrB located in the inner membrane, and the periplasmic AcrA, which bridges these two integral membrane proteins. The AcrAB-TolC efflux pump is able to vectorially transport a diverse array of compounds with little chemical similarity, and accordingly confers resistance to a broad spectrum of antibiotics. Homologous complexes are found in many Gram-negative species, including pathogens of animals and plants. Crystal structures are available for the individual pump components[2-7] and these have provided insights into substrate recognition, energy coupling and the transduction of conformational changes associated with the transport process. How the subunits are organised in the pump, their stoichiometry and the details of their interactions are not known and are under debate. In this manuscript, we present the pseudoatomic structure of a complete multidrug efflux pump in complex with a modulatory protein partner[8]. The model defines the quaternary organization of the pump, identifies key domain interactions, and suggests a cooperative process

Correspondence and requests for materials should be addressed to B.F.L (bfl20@cam.ac.uk) or D.D. (dd339@cam.ac.uk).

Author contributions D.D., W.C. and B.F.L. designed the experiments; D.D. and N.R.J. purified and crystallized AcrBZ complexes. D.D. and B.F.L. solved the crystal structure of AcrBZ complexes. D.D., N.R.J. and E.K. purified AcrABZ-TolC complexes. Z.W., J.E.V. and W.C. obtained and analysed the single particle cryo-electron microscopy data. D.D. and B.F.L. devised a model of AcrABZ-TolC based on cryo-EM map. T.O. and R.V conducted MIC and efflux assays of AcrABZ-TolC pump. D.D., J.E.V., W.C. and B.F.L. analysed results. All authors contributed to writing the manuscript.

Author Information Atomic coordinates and structure factors for the reported crystal structures have been deposited with the Protein Data Bank under accession codes 4C48 (AcrB/AcrZ/DARPin) and 4CDI (AcrB/AcrZ). The EM map has been deposited in the EMDataBank under accession code EMD-5915.

The authors declare no competing financial interests.

Europe PMC Funders Author Manuscripts

for channel assembly and opening. These findings illuminate the basis for drug resistance in numerous pathogenic bacterial species.

Recently, a small protein of 49 residues, AcrZ, has been identified in genetic screens as a binding partner of AcrB that affects substrate preference[8]. A mutant strain of *E. coli* lacking AcrZ is sensitive to some, but not all, antibiotics that are exported by the AcrAB-TolC pump. AcrZ is conserved in many enterobacterial lineages, suggesting that modulation by small proteins may be a recurring theme in the RND protein family to which AcrB belongs.

To investigate their interaction, AcrB was coexpressed with AcrZ carrying a C-terminal histidine tag. The partner proteins copurified through Ni^{2+} affinity and size-exclusion chromatography (Extended Data Figure 1A) and co-crystals of the AcrBZ complex were obtained. Additionally, better-diffracting co-crystals were obtained of a ternary complex formed with a designed ankyrin-repeat protein (DARPin) used in previous studies for co-crystallization with AcrB[9] (Extended Data Figures 1B,C; Extended Data Table 1). Electron density corresponding to AcrZ was apparent in the early, unbiased maps (Extended Data Figure 2). AcrZ folds into a long, predominantly hydrophobic α-helix that fits into a wide groove in the transmembrane domain of AcrB (Figure 1A,B; Extended Data Figure 2). The AcrBZ complex overlays well with the previously reported structure of AcrB bound to another potential partner, YajC[10] (Extended Data Figure 3A). The helical axis of AcrZ is inclined by nearly 45° with respect to the normal vector of the lipid bilayer, and although this is an unusual extent of inclination for a transmembrane α-helix, it optimizes the interfacial complementarity. The interfacial residues are well conserved amongst the identified homologues of AcrZ, suggesting that analogous interactions are likely to occur for other RND family proteins (Extended Data Figure 3B,C). AcrZ residues 1-46 could be modelled, revealing that the N-terminus is in the periplasm and the C-terminus is in the cytoplasm, where it interacts with the hydrophilic surface of AcrB near the membrane (Figure 1B). It seems possible that the reported effects of AcrZ on drug sensitivity[8] might originate form the allosteric modulation of AcrB activity by AcrZ.

To stabilize the complete pump assembly, constructs were prepared in which the components were fused (Extended Data Figure 4A). Based on the crystal structure of the AcrBZ complex, a construct was designed in which AcrA is fused through a flexible linker to the N-terminus of AcrZ, which was predicted to leave the individual structures unperturbed and to permit localization of AcrA to the periplasm while allowing AcrZ to cross the inner membrane with the correct topology and preserving its interactions with AcrB. This fusion harbours a histidine tag on the C-terminus of AcrZ to facilitate Ni^{2+} affinity purification of the fusion protein. In a second engineered construct, we identified loops in the periplasmic domain of AcrB where AcrA could be inserted with flexible linkers. Both the AcrA-AcrZ-His_5 and AcrA-AcrB fusions were stable during overexpression and purification.

One current debate in the field is the compositional stoichiometry of the pump, with evidence favouring a 3:6:3 ratio for AcrB:AcrA:TolC[11-16]. To enable the assembly of such a complex, we explored the coexpression of the fusion pairs AcrA-AcrB and AcrA-AcrZ-His_5. In the course of isolating the coexpressed recombinant proteins, we observed that the

Europe PMC Funders Author Manuscripts

AcrA-AcrZ-His_5 fusion copurified with both the AcrA-AcrB fusion and endogenous TolC. We subsequently designed coexpression vectors comprising fusion proteins of AcrA-AcrB, AcrA-AcrZ-His_5 and TolC and found that the proteins remained associated during purification (Extended Data Figure 4B). MIC (Minimum inhibitory concentration) and drug efflux assays of the AcrAB and AcrAZ fusion proteins show that the engineered pump retains partial activity(Extended Data Figure 5).

The assembly was further purified by the 'GraFix' method[17] and analysis of the fractions by negative-stain electron microscopy readily led to the identification of drumstick-shaped particles that matched the expected size and shape of the pump (Extended Data Figure 6A). The crosslinked particles were subsequently imaged using electron cryo-microscopy (cryo-EM), which shows images of isolated and aggregated particles (Figure 2A). Initial 3-D reconstruction was carried out using EMAN2[18] without any imposed symmetry (Extended Data Figure 6B), which suggested the presence of at least 3-fold symmetry. As TolC and AcrB are known to be homotrimers, a subsequent 3-fold symmetry enforced map was independently produced (Extended Data Figure 6C). We then used RELION software [19] to refine the particle classification and orientation determination, which improved the map greatly. The resolution of the final map was estimated to be ~16 Å (Extended Data Figure 7A). This map was validated by a tilt-pair analysis (Extended Data Figure 7B), which is considered to be a best practice to assess the correctness of a low resolution cryo-EM map [20].

The quality of this final density map was sufficient to permit docking of the crystal structures of TolC, AcrA and the AcrBZ complex with only small movements in the flexible linker regions between the domains of AcrA (Figure 2B; materials and methods). Following sequential fitting of AcrA, AcrBZ and TolC into the cryo-EM map, the final model has good agreement with the density envelope (Figure 2B,C; Extended Data Figure 8A). The transmembrane portion of TolC is enclosed in a torus that resembles the detergent shell observed for aquaporin in the same detergent used in this study, namely *n*-dodecyl-β-D-maltopyranoside (DDM) [21]. The detergent also forms a layer around the transmembrane portion of AcrB (Figure 2B,C).

One salient observation of our model is that there is no direct interaction between TolC and AcrB in the assembly, in contradiction to earlier models[3,22]. Instead, the two proteins are bridged in the periplasm entirely through AcrA. This is consistent with *in vivo* crosslinking and pull-down assays, which indicated that AcrA interacts with AcrB and TolC independently, while no interaction was observed between AcrB and TolC[23]. Our model also accounts for thermodynamic measurements suggesting that the pairwise interactions of AcrA/AcrB and AcrA/TolC occur spontaneously, whereas that between AcrB and TolC does not[24]. The organization of the AcrA/TolC subassembly is in agreement with the dimensions of the homologous MexA-OprM complex from *Pseudomonas aeruginosa*[24,25].

Our model shows that the assembly comprises an AcrB trimer, an AcrA hexamer, and a TolC trimer. This is in accord with the 3:6 stoichiometry of the homologous CusA/CusB heavy metal efflux complex[15]. The hexameric assembly of AcrA resembles that of the homologous MacA (Figure 3A, B)[16]. The α-helical coiled coils (or 'hairpins') of AcrA pack

into a cylinder that interacts with the periplasmic ends of the α-helical coiled coils portion of TolC. As TolC has an internal structural repeat, there are six quasi-equivalent contact surfaces that interact with the AcrA hairpins (Figure 3A, Extended Data Figure 8B).

The membrane proximal domain and β-barrel domain of AcrA are involved in defined interactions with AcrB (Figure 3A). One protomer of AcrA bridges the upper regions of subdomains PC1, PC2 and DC of AcrB (protomer 1 in Figure 3A); this interaction is similar to that between CusA and CusB (Figure 3C). However, the adjacent protomer of AcrA (protomer 2 in Figure 3A) interacts with AcrB in a different manner: here, the membrane-proximal domain of AcrA shifts towards the PN2 subdomain of AcrB so that only the upper regions of PN2 and DN contact AcrA. The lipoyl domains of AcrA principally interact with each other to form a channel that is closed to the periplasm and make no predicted interactions with either AcrB or TolC.

The side-by-side packing of the β-barrel, lipoyl and helical hairpin domains of the six AcrA protomers generates a funnel-like structure with a sealed central channel along the three-fold axis. A chamber is formed by the β-barrel and lipoyl domains of AcrA, and the bottom of the chamber opens into the funnel of AcrB. The chamber is partially constricted near the middle of the lipoyl domain (Figure 2C; Extended Data Figure 8A). It then continues to a channel created by the helical hairpin domains, with a cogwheel shape at the end of these domains, like that of MacA (Figure 3A,B). The modelled docking of the membrane-proximal domain of AcrA onto the surface of AcrB is consistent with the disruptive behaviour of mutants at that interface[26,27].

A cross section through the reconstruction reveals a conduit that is open to the cell exterior and runs from the transmembrane β-barrel of TolC, through the TolC periplasmic domain, and continues all the way to the funnel-shaped canyon in the periplasmic domain of AcrB (Figure 2C). The cross section indicates that the channel is sealed off from the periplasm and cytoplasm, and the components in the pseudoatomic model shown in Figure 2B pack efficiently to leave no gaps. The conduit is the likely exit pathway for efflux of substrates, which will be delivered into this chamber through successive opening and closing of ligand-binding pockets in AcrB, adjacent to the apex of the funnel-shaped periplasmic canyon.

In isolation, TolC assumes a ‘closed’ resting state in which its periplasmic domain tapers to a near close, but to be accommodated in the continuous channel seen in the cryo-EM model, TolC must switch to an ‘open’ state[28,29] (Figure 2A; Extended Data Figure 8B). The opening of TolC must result from its direct interactions with the α-helical hairpins of AcrA. In this scenario, AcrB provides a platform for the proper assembly of hexameric AcrA suitable for presentation to TolC and opening of the channel. The AcrAB-TolC assembly forms *in vivo* without the requirement for substrates or proton-motive force[30], suggesting that exogenous energy may not be required to open TolC in the context of the assembled pump. It seems likely that TolC remains open throughout the transport cycle, and we propose that the dilation of TolC from the closed to the open state is driven by both chelate cooperativity (due to the hexameric organization of AcrA) and allosteric cooperativity (associated with the breaking of interprotomer interactions in TolC).

The structure of the efflux pump presented here is likely to be similar to homologous assemblies in pathogenic species of humans such as *Vibrio cholera*, *Pseudomonas aeruginosa*, *Neisseria gonorrhoeae* and *Salmonella enterica*. The question naturally arises as to how it might be feasible to counter the actions of drug efflux in the treatment of threatening bacterial infections. It seems paradoxical that a compound might exist that would achieve this, when the pump is well crafted to handle diverse compounds. Perhaps the protein-protein contacts that mediate the assembly might be favourable targets for such approaches.

METHODS

Construction of vectors for overexpression of AcrBZ and AcrABZ-TolC complex

The *acrZ* gene was generated by PCR from genomic DNA of *E. coli* W3110 strain using primers AcrZNcoI_F: 5′- TGG CCA TGG GCT TAG AGT TAT TAA AAA GTC TGG TAT TCG CCG TAA TCA TGG -3′ and AcrZHis5SalI_R: 5′- GAC GTC GAC TCA GTG GTG GTG GTG GTG GTG ATG ATT TTG TCC GGG CTG GTC TTT TTT ACC -3′. The **pRSFduet-1-*acrZ*$_{His5}$** vector was constructed by subcloning the fragment of *acrZ-His*$_5$, bounded by *NcoI* and *SalI* sites, into the MCS of expression vector pRSFDuet-1.

The pET21a-*acrB*$_{His6}$ vector was constructed by subcloning the fragment of *acrB*, bounded by *NdeI* and *XhoI* sites, into the MCS of expression vector pET21a. The **pET21a-*acrB*$_{\Delta His}$** was constructed by site-directed mutagenesis using pET21a-*acrB*$_{His6}$ as template and primers AcrB_CF: 5′-TGA AGA TAT CGA GCA CAG CCA TAC TGT CGA TTG AGA TCC GGC TGC TAA CAA AGC CC -3′ and AcrB_CR: 5′- GGG CTT TGT TAG CAG CCG GAT CTC AAT CGA CAG TAT GGC TGT GCT CGA TAT CTT CA -3′.

The *acrA* gene was amplified using primers AcrANcoI_F: 5′-TGG CCA TGG GCA ACA AAA ACA GAG GGT TTA CGC CTC TGG CG -3′ and AcrAGSx3_R: 5′-TGG CCA TGG ATC CGC CGC CAC CAG AGC CAC CAC CGC CGC TCC CAC CGC CAC CAG ACT TGG ACT GTT CAG GCT GAG CAC C-3′, to add a poly-GlySer linker to the C-terminus and a *NcoI* site at both ends. The *Nco I* bounded *acrA-polyGS* was subcloned into the *Nco I* site of pRSFduet-1-*acrZ*$_{His5}$, resulting in the construct pRSFduet-1-*acrA-polyGS-acrZ*$_{His5}$. The *tolC* gene was amplified using primers TolCinf_F: 5′- AAG GAG ATA TAC ATA TGA AGA AAT TGC TCC CCA TTC TTA TCG GCC-3′ and TolC1392inf_R: 5′- TTG AGA TCT GCC ATA TGT CAA TCA GCA ATA GCA TTC TGT TCC GGC GT-3′. The PCR product was then inserted into the *Nde I* site of pRSFduet-1-*acrA-polyGS-acrZ*$_{His5}$ using In-Fusion cloning method (Clontech), generating the construct **pRSFduet-1-*acrA-polyGS-acrZ*$_{His5}$*-tolC*$_{1392}$.**

A *BamH I* site was inserted into *acrB* by site-directed mutagenesis using pET21a-*acrB*$_{\Delta His}$ as template and primers AcrB_D328F: 5′-CTG AAA ATT GTT TAC CCA TAC GAC GGA TCC ACC ACG CCG TTC GTG AAA -3′ and AcrB_D328R: 5′-TTT CAC GAA CGG CGT GGT GGA TCC GTC GTA TGG GTA AAC AAT TTT CAG-3′, resulting in a construct pET21a-*acrB*$_{\Delta His}$*BamHI*$_{328}$. The *acrA* gene was amplified using primers AcrA_25GSF: 5′-GGA TCC GGT GGG AGC GGT GGC GGC GGT AGT GGC GGT GGT GGC TCT TGT GAC GAC AAA CAG GCC CAA CAA GG -3′ and AcrAGSx3_R:

5′-GGA TCC GCC GCC ACC AGA GCC ACC ACC GCC GCT CCC ACC GCC ACC AGA CTT GGA CTG TTC AGG CTG AGC ACC-3′, to add a poly-GlySer linker to both ends of *acrA*. The resulting DNA fragment was amplified again using primer AcrA Infusion_Forward: 5′- CCC ATA CGA CGG ATC CGG TGG GAG CGG TGG CGG CGG TA-3′ and AcrA Infusion_Reverse: 5′-ACG GCG TGG TGG ATC CGC CGC CAC CAG AGC CAC CAC C-3′. The DNA fragment was then inserted into the *BamH I* site of pET21a-$acrB_{\Delta His}BamHI_{328}$ using In-Fusion cloning method, generating the construct **pET21a-$acrB_{328}$-polyGS-acrA-polyGS-$acrB_{329}$**.

Overexpression and purification of the AcrBZ and the AcrBZ/DARPin complexes

The constructs pET21a-$acrB_{\Delta His}$ and pRSFDuet-1-$acrZ_{His5}$ were transformed into *E. coli* strain C43(DE3) Δ*acrAB* [31]. The C-terminal histidines of AcrB were substituted to prevent nonspecific association with metal affinity matrix. Cells were grown in 2 × YT medium with 100 μg·ml^{-1} carbenicillin and 50 μg·ml^{-1} kanamycin at 37 °C until the culture reached an absorbance, at 600 nm, of 0.5–0.6 and was then induced by the addition of 0.5 mM isopropyl 1-thio-β-D-galactopyranoside (IPTG) at 18 °C overnight. Cell pellets were resuspended in lysis buffer (400 mM sodium chloride, 20 mM Tris-HCl, pH 8.0) with 1 tablet/50 ml EDTA-free protease inhibitor cocktail tablets, 5 U·ml^{-1} DNase I and 5 mg·ml^{-1} lysozyme, and the mixture was stirred at 4 °C for 1 h to digest the cell wall. The cells were lysed using a homogenizer (EmulsiFlex) at 15,000 psi for eight passages. Cell debris was pelleted by centrifugation at 9,000 × ***g*** for 30 min. Cellular membrane was pelleted by ultracentrifugation at 125,755 × ***g*** for 3 h.

Membrane pellets were resuspended in lysis buffer with protease inhibitors and were solubilized by adding 1.5% n-dodecyl-β-D-maltopyranoside (DDM) and stirring at 4 °C for 3 h. Debris was pelleted by ultracentrifugation at 125,755 × ***g*** for 30 min. Imidazole was added to the membrane solution to a final concentration of 10 mM. Histidine tagged AcrBZ complex was purified by nickel affinity chromatography using a HiTrap chelating column (GE Healthcare Life Sciences) equilibrated with GF buffer (400 mM sodium chloride, 20 mM Tris-HCl, pH 8.0, 0.05% DDM) containing 20 mM imidazole. The column was washed with 50 mM and 75 mM imidazole added to GF buffer, respectively. Purified AcrBZ complex was eluted with 500 mM imidazole in GF buffer, concentrated and loaded onto a Superose 6 column equilibrated with GF buffer. Fractions containing purified AcrBZ complex were pooled and concentrated to 15-20 mg ml^{-1} using a VIVA Spin column (MWCO=100 kDa) and dialysed overnight against sample buffer (10 mM HEPES pH 7.5, 50 mM sodium chloride, 0.03% DDM) using a 100 kDa MWCO dialysis membrane to decrease the detergent concentration.

The DARPin gene was synthesized and protein was overexpressed and purified as described [32]. Purified DARPin and AcrBZ complex were mixed at a molar ratio of 1:2 (AcrBZ monomer:DARPin monomer). The mixture was diluted with GF Buffer-II (20 mM Tris-HCl, pH 7.5, 150 mM sodium chloride, 0.03% DDM) to a concentration of 2-3 mg/ml, incubated at 4°C overnight, then concentrated to 0.5 ml using a VIVA Spin column (MWCO=100 kDa) and loaded onto a Superose 6 column equilibrated with GF buffer-II. Fractions containing purified AcrBZ/DARPin complex were pooled and concentrated to

15-20 mg ml^{-1} using a VIVA Spin column (MWCO=100 kDa) and dialysed overnight against sample buffer using a 100 kDa MWCO dialysis membrane; the final concentration is 10-15 mg ml^{-1}.

Crystallization of AcrBZ and AcrBZ/DARPin

The AcrBZ and AcrBZ/DARPin complexes were diluted to 10 mg ml^{-1} using sample buffer. 9 mM n-octyl-β-D-thioglucopyranoside (90 mM) was mixed with AcrBZ complex before the crystallisation trials. The AcrBZ crystals were grown at 20 °C using the hanging-droplet vapour diffusion method by mixing 4 μl of AcrBZ complex with 2 μl of reservoir solution (100 mM tricine pH: 7.4, 50 mM lithium sulphate, 5 mM cadmium chloride hydrate, 7 % PEG 3000, 10% glycerol). The AcrBZ/DARPin complex was incubated with puromycin at 1 mM for 3 hours at 4°C before crystallisation trials. Crystals were grown at 20 °C using the sitting-droplet vapour diffusion method by mixing 400 nl of AcrBZ/DARPin complex with 200 nl of reservoir solution (100 mM HEPES, pH 7.5, 10 mM $MgCl_2$ and 12% (w/v) PEG 3350). Crystals appeared 24 hours after setting-up the crystallization trials and reached maximal size in 1 week. The crystals were transferred briefly into reservoir solution supplemented with 25% glycerol as cryoprotectant before flash freezing in liquid nitrogen.

Crystallographic data collection and structure refinement

Datasets were collected using beamlines I04-1 and I24 at Diamond Light Source. The diffraction data were processed using X-ray Detector Software (XDS) [33] and scaled using SCALA [34]. Structures were solved by molecular replacement using Phaser with chain A of AcrB (PDB 4DX5) [35] and refined using Crystallography and NMR System (CNS) [36,37], PHENIX [38], and REFMAC5 [39] with reference structure restraints[40]. Coot was used for modelling[41]. Data collection and refinement parameters are presented in Extended Data Table 1.

Both the AcrBZ and AcrBZ/DARPin complexes crystallised in space group R32. A monomer of AcrB trimer occupies the asymmetric unit, with one AcrZ bound in crystals of both complexes. Maps calculated from molecular replacement using only the AcrB protomer revealed clear electron density for AcrZ in both complexes (see Extended Data Figure 2). For the AcrBZ/DARPin complex, unbiased density was also present that could fit the DARPin model. Density was also apparent that matched the modelled detergent and acyl chains in the 1.9 Å resolution structure of *E. coli* AcrB [35] (PDB ID: 4DX5). These were included in the model, as well as additional acyl chains that were located mostly in the intra-protomer space in the transmembrane region of AcrB. For both AcrBZ and AcrBZ/DARPin complexes, the AcrB trimer is formed through crystallographic symmetry, so that any potential non-equivalence of the protomers are consequently lost.

Expression and purification of the efflux pump assembly

The constructs pET21a-$acrB_{328}$-*polyGS-acrA-polyGS-*$acrB_{329}$ and pRSFduet-1-*acrA-polyGS-*$acrZ_{His5}$-$tolC_{1392}$ were transformed into *E. coli* strain C43(DE3)Δ*acrAB*. The procedure for overexpression and purification of AcrABZ-TolC is similar to that of AcrBZ, with minor modification: Cells were induced with 0.25 mM IPTG at 20 °C overnight, harvested and resuspended in lysis buffer-II (20 mM Tris.HCl, pH 7.5, 400 mM NaCl) for

membrane preparation. Cellular membrane was solubilized with 1.5% DDM in lysis buffer-II. The AcrABZ-TolC complex purified by nickel affinity chromatography was loaded onto a Superose™ 6 column equilibrated with GF buffer-III (50 mM HEPES pH 7.5, 400 mM NaCl, 0.03% DDM). Fractions containing purified AcrABZ-TolC complex were pooled and concentrated to 1 mg ml^{-1} using a VIVA Spin column (MWCO=100 kDa).

Transport assays

Transport activity was measured as described[42] with some modifications. Plasmids were propagated in the triple knockout *E. coli* strain MC*ΔtolCΔacrAB* [43,44], a derivative of *E. coli* MC1061 converted to a (DE3) lysogen. All experiments employed basal levels of protein expression without induction with IPTG. Cells were grown in LB-Broth Miller (Formedium) containing the appropriate antibiotic(s) with shaking at 37 °C until an OD_{660} of 0.5 was reached. The cells were harvested by centrifugation at 3000 × ***g*** for 10 min at 4°C, then washed three times by resuspension in 50 mM potassium phosphate buffer, pH 7.0 containing 5 mM $MgSO_4$ and sedimented by centrifugation at 3000 × ***g*** for 10 min at 4°C. The cells were then resuspended in the same buffer to an OD_{660} of 0.5 and incubated for 3 min at room temperature (25°C) in the presence of 25 mM glucose to energise the cells. The fluorescence measurement was started, and 60 s later 2 μM ethidium bromide or 0.25 μM trimethylammonium-diphenylhexatriene (TMA-DPH) was added. The fluorescence was followed as a function of time in a PerkinElmer LS 55B fluorimeter. Excitation and emission wavelengths and excitation and emission slit widths were 500, 580, 5 and 10 nm respectively for ethidium bromide; and 350, 425, 5 and 5 nm respectively for TMA-DPH. Initial substrate transport rates were determined between 85 to 185 s and 75 to 95 s for ethidium bromine and TMA-DPH respectively. Assays were performed twice in a day for three separate days, with different cell preparations used each day.

GraFix preparation of the efflux pump assembly

The GraFix procedure for AcrABZ-TolC complex was carried out as described [45,46]. Gradients for GraFix were generated by mixing GraFix Buffer-I (50 mM HEPES pH 7.5, 400 mM NaCl, 0.03% wt/v DDM, 10% v/v glycerol) and GraFix Buffer-II (50 mM HEPES pH 7.5, 400 mM NaCl, 0.03% w/v DDM, 30% v/v glycerol, 0.15% v/v glutaraldehyde) using a gradient mixer (Gradient Master 107, BioComp Instruments), following the manufacturer's recommendations for determining the parameters. 100 pmol of AcrABZ-TolC complex was loaded on the top of the buffering cushion. Ultracentrifugation was carried out at 111,845 × ***g***, 4 °C for 18 hours (SW60 rotor, Beckmann). Following centrifugation, the gradients were fractionated at 4°C by using a capillary to pump the gradient out from bottom to top, taking fractions of 200 µl. The same fractions from different centrifuge tubes were pooled respectively. Glycine (1 M, pH 7.5) was added to the fractions to a final concentration of 80 mM to quench further crosslinking, and the mixtures were concentrated to 200 µl using a VIVA Spin column (MWCO=100 kDa). The concentrated protein samples were diluted to 1 ml using GF buffer-III, and were concentrated to 100 µl again to decrease the concentration of glycerol. The AcrABZ-TolC samples were frozen in liquid nitrogen and stored at −80° C.

Europe PMC Funders Author Manuscripts

Negative stain electron microscopy

Continuous carbon electron microscopy grids (Agar Scientific) were glow discharged. Sample adsorption was achieved by placing the grid carbon side down on a 10 μL drop of protein solution at a concentration of approximately 10 μg ml^{-1}. Adsorption times were determined empirically. After blotting to dryness, the grid was washed by placing it onto a drop of deionised H_2O for 5 s, blotted dry, and then repeated. The protein was stained by transferring the grid to a drop of 2% wt/v uranyl acetate for 30 s, then dried and stored at room temperature. The sample was then imaged at 20,000× magnification and 120 keV in a FEI Tecnai G^2 microscope at the Multi Imaging Centre, University of Cambridge.

Cryo-EM specimen preparation and data collection

Samples were embedded in vitreous ice as the following. A 2.0 μl aliquot at approximately 2 mg/ml was applied onto holey carbon film supported by a 200-mesh R1.2/1.3 Quantifoil grid (Quantifoil) that had been previously washed and glow discharged. The grid was blotted and rapidly frozen in liquid ethane using a Vitrobot IV (FEI) with constant temperature and humidity during the process of blotting, and the grid was stored in liquid nitrogen before imaging. All grids were screened on a JEM3200FSC electron cryo-microscope (JEOL) operated at 300 kV, spot size = 2, condenser aperture = 70 μm, objective aperture = 60 μm, and energy slit of the in-column filter of 20 eV. Images were recorded with a direct detection device (DDD) (DE-12 3kx4k camera, Direct Electron, LP) operating in movie mode at recording rate of 25 raw frames per second. At a 20,000× microscope magnification (corresponding to a calibrated sampling of 2.47 Å/pixel) and a dose rate of 25 electrons/s/$Å^2$ were used to acquire data for each specimen area with a total exposure time of 2 seconds. A total of 1,281 DDD images using movie frame mode were collected with a defocus range of 2–4 μm.

Cryo-EM data processing, resolution evaluation

Particle images were manually boxed with the EMAN2 program *e2boxer.py* [47] with a box size of 256 × 256 pixels using the averaged sum of 48 raw frames per specimen area. The final frame average was computed from averages of every five consecutive frames to correct for the specimen movement during exposure similar to the procedure previously described[48]. The particle intensity in each frame was weighted according to a radiation damage model (courtesy of B. Bammes of Direct Electron, LP). Defocus of the particles in each frame average was determined by EMAN2 program *e2ctf.py*[49]. The first reconstruction was done without any symmetry imposition or any initial model, using EMAN2 [47]. We started with 12,000 particle images and 8,400 particle images were selected manually according to the similarity in appearance to the class averages. The first map without any symmetry imposition appeared to have a 6-fold symmetry (Extended Data Figure 6B), which justified applying a 3-fold symmetry enforcement (Extended Data Figure 6C). The symmetry-free and symmetry-imposed map look similar except for a slight difference in contrast. Then, we used RELION [50] to perform two additional steps of particle orientation refinement of the 8,400 selected particle images. Using the EMAN2 generated map (Extended Data Figure 7A), low pass filtered to 60Å, we preformed a particle orientation refinement by RELION with search angle of 7.5 degrees for 14 iterations and subsequently

with an angular sampling of 1.8 degrees for 11 iterations. The resolution of the resulting map is 21Å based on 0.143 FSC criterion (Extended Data Figure 7A). Next, this map was sharpened [47] and low pass filtered to 30Å before preforming a second round of particle orientation refinement by RELION with an angular sampling of 1.8 degrees for 8 iterations. The resolution of final map is estimated to be 16Å by 0.143 FSC criterion (Extended Data Figure 7A). The final map displayed in Figure 2 B, C has been sharpened and filtered to 16Å.

Cryo-EM map tilt pair validation

To further validate the cryo-EM map (Figure 2B), we carried out tilt-pair analysis[51] of the AcrABZ-TolC complex. Pairs of images were recorded on a JEM2010F electron microscope at a magnification of 30,000× with a relative tilt of 10 degrees, along a known axis. Each pair of particle images thus has a known experimental relative tilt. We then determined the orientation of each image in the pair using the final-reconstructed map as a reference. The relative tilt between these computed orientations should match the experimental tilt. Each point in Extended Data Figure 7B represents one pair of particles in the tilt pair, with radius representing computed relative tilt, and azimuth representing tilt angle. Ideally all points would lie in exactly the same location; however, there is always some uncertainty in orientation determination, exacerbated in this case by radiation damage in the second image of the tilt pair and the strong pseudo hexagonal symmetry. As previously observed [52], if the map is incorrect, the relative angles will not correlate at all, and produce a nearly random distribution over the sphere. A clear cluster as observed in our case is an indication of successful validation, and our experimental tilt angle of 10.44 degrees is an extremely good match with the experimental tilt of 10 degrees. The presence of some points at mirrored positions across the origin is an indication of weak handedness in the map, meaning the map and its mirror image is difficult to distinguish at this resolution in some orientations.

Model docking

The merged map was low pass filtered before rigid body docking of crystal structures using Coot and UCSF Chimera[53] (http://www.cgl.ucsf.edu/chimera). The symmetric partially opened model of TolC was used to prepare a fully opened model (PDB ID: 2XMN)[54]. A homologous model of the inner sets of coiled coils was devised based on the outer sets of coiled coils, which was used to replace the inner sets of coiled coils. The uncoiling movement of the inner sets of coiled coils produced a fully opened TolC [55].

The β-barrel domain, lipoyl domain and α-helical hairpin domain of AcrA protomer were modelled with chain C in the asymmetric unit of the crystal structure of AcrA (PDB ID: 2F1M)[56]. A homology model of the membrane proximal domain of AcrA was devised based on the structure of MexA (PDB ID: 2V4D)[57].

The individual domains of AcrA were fitted into the cryo-EM reconstruction using Coot, according to the features of the cryo-EM map and knowledge of hexameric MacA assembly (PDB ID: 3FPP and 4DK0). The closed state TolC (PDB ID: 1EK9), partially opened (PDB ID: 2XMN) and fully opened model of TolC were fitted into the cryo-EM reconstruction, respectively. The AcrBZ trimer, the TolC trimer and the AcrA hexamer were treated as

individual rigid bodies. These three rigid bodies were automatically fitted into the cryo-EM map by sequential fitting using Chimera. The AcrABZ-TolC model generated by Chimera was slightly adjusted manually to optimize the local fit into the density using Coot[41]. The cross-correlation coefficient for fitting the AcrABZ-open TolC model to the map is 0.924 and was calculated using the *Fit in Map* function of Chimera.

Extended Data

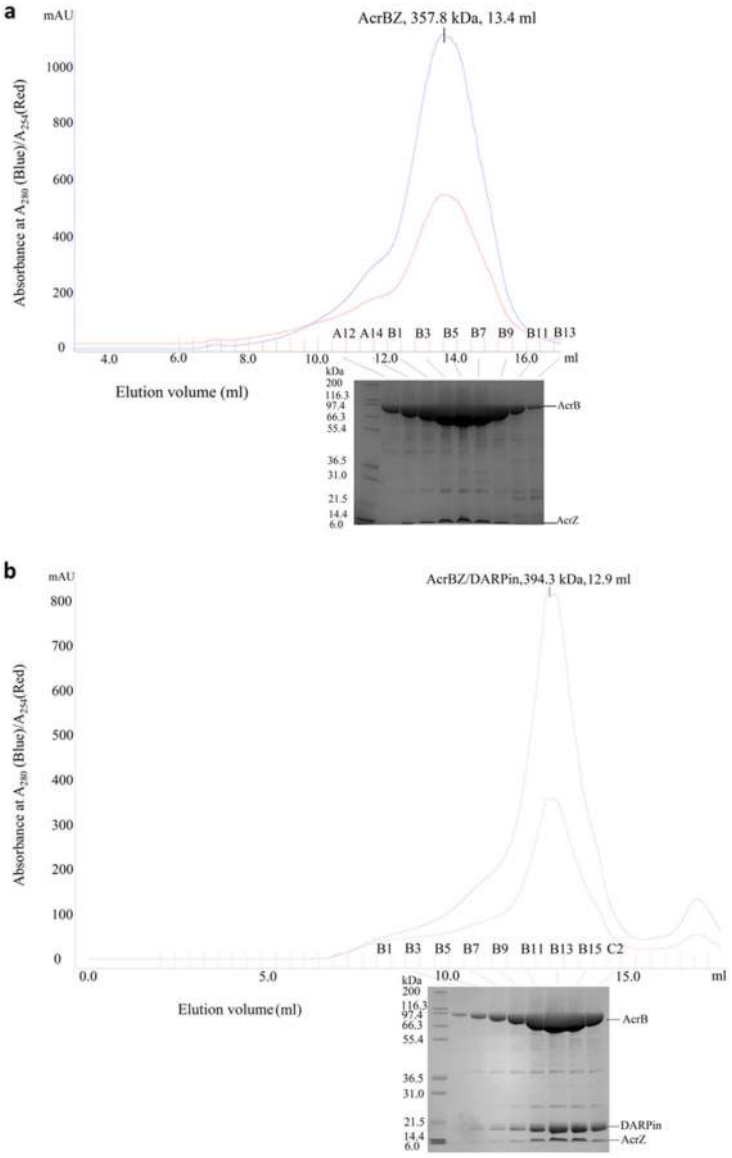

Extended Data Figure 1.

Co-purification of the AcrBZ and AcrBZ/DARPin complexes. A) Gel filtration profile of AcrBZ complex and SDS-PAGE analysis of the peak fractions. B) Gel filtration profile of the AcrBZ/DARPin complex and SDS-PAGE analysis. The proteins were enriched by Immobilised metal affinity chromatography (IMAC, results not shown) before the size exclusion chromatography step. The AcrZ has a heptahistidine tag on the C-terminus as an

Europe PMC Funders Author Manuscripts

IMAC affinity tag, and the C-terminal histidines of AcrB have been removed to prevent its binding to the matrix. Standard proteins Thyrogloblin, 669 kDa, and Aldolase, 158 kDa, (Bio-Rad) eluted from the same column at volumes of 11.4 and 14.7 mL respectively. The figure is related to Figure 1 in the main text.

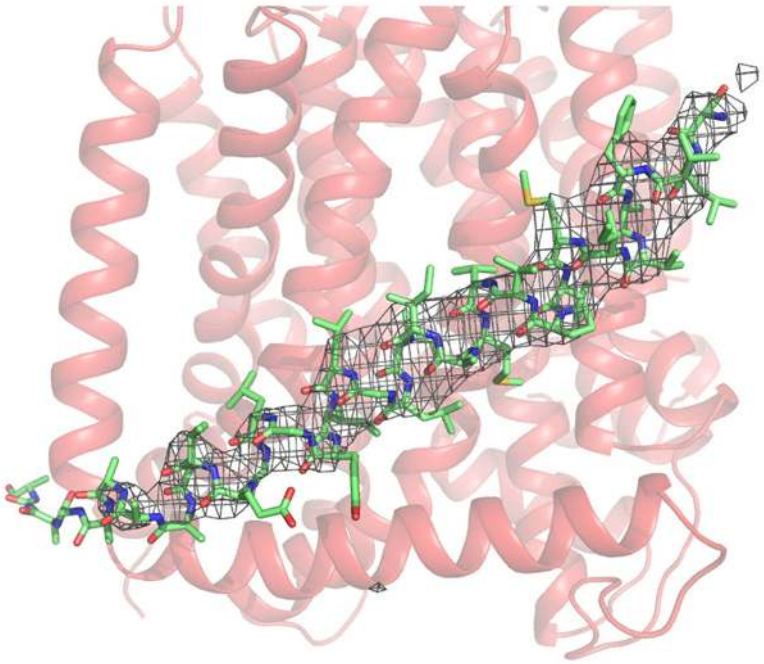

Extended data Figure 2.

Validation of the AcrBZ crystal structure. An AcrB protomer taken from the refined structure of the AcrBZ/DARPin complex at 3.3 Å was used in molecular replacement of the 3.7 Å data of the AcrBZ complex (Extended Data Table 1). The model of AcrB without AcrZ was refined with REFMAC[40] jelly-body and reference structure restraints, and a difference map calculated in which AcrZ does not contribute to the phases. The figure shows the positive features of the difference map in the vicinity of AcrZ (green carbon atoms) taken by superposing the AcrB protomers from the AcrBZ/DARPin and AcrBZ (red) structures. The unbiased map shows the presence of AcrZ and indicates that the presence of the DARPin does not disrupt the interactions with AcrB.

The model of the AcrBZ/DARPin complex at 3.3 Å was refined without the AcrZ to generate a simulated annealing omit map, which confirmed the location of the AcrZ (not shown). The figure is related to Figure 1 in the main text.

Europe PMC Funders Author Manuscripts

Europe PMC Funders Author Manuscripts

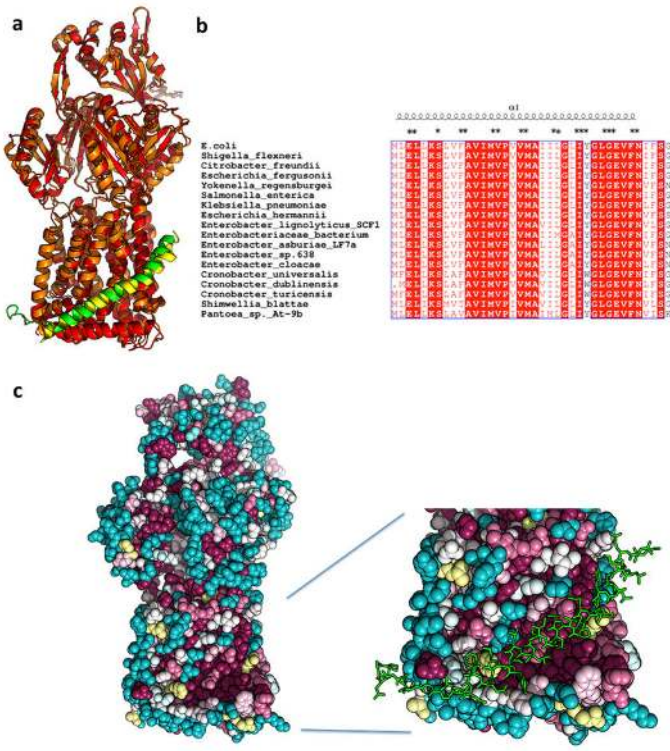

Extended data Figure 3.

The AcrBZ complex resembles AcrB-YajC, and AcrBZ interactions involve conserved residues. (A) Superposition of AcrB-YajC (orange and yellow; PDB ID: 2RDD) onto AcrBZ (red and green). The figure supports Figure 1 of the main text. We were not able to identify an interaction between AcrB and C-terminal-histidine-tagged YajC from *E. coli*, suggesting that the interaction is less avid than the AcrB/AcrZ pairing (data not shown). It is interesting to note that the contacting surface is also conserved in another RND family transporter, SecDF, involved in protein translocation and membrane insertion[58]. It thus seems likely that SecDF might be modulated by a similar helical peptide. Indeed, YajC forms a complex with SecDF[59,60] and could play an allosteric role in the process. (B) Sequence conservation of AcrZ. The secondary structure is annotated at the top and asterisks indicate residues that directly contact AcrB. (C) Sequence variation of the surface of AcrB homologues, showing conservation of the surface that contacts AcrZ. The figure on the right includes the bound AcrZ in stick representation (green). The colour spectrum ranges from purple (most conserved) to blue (least conserved). This figure was made with ConSurf [61].

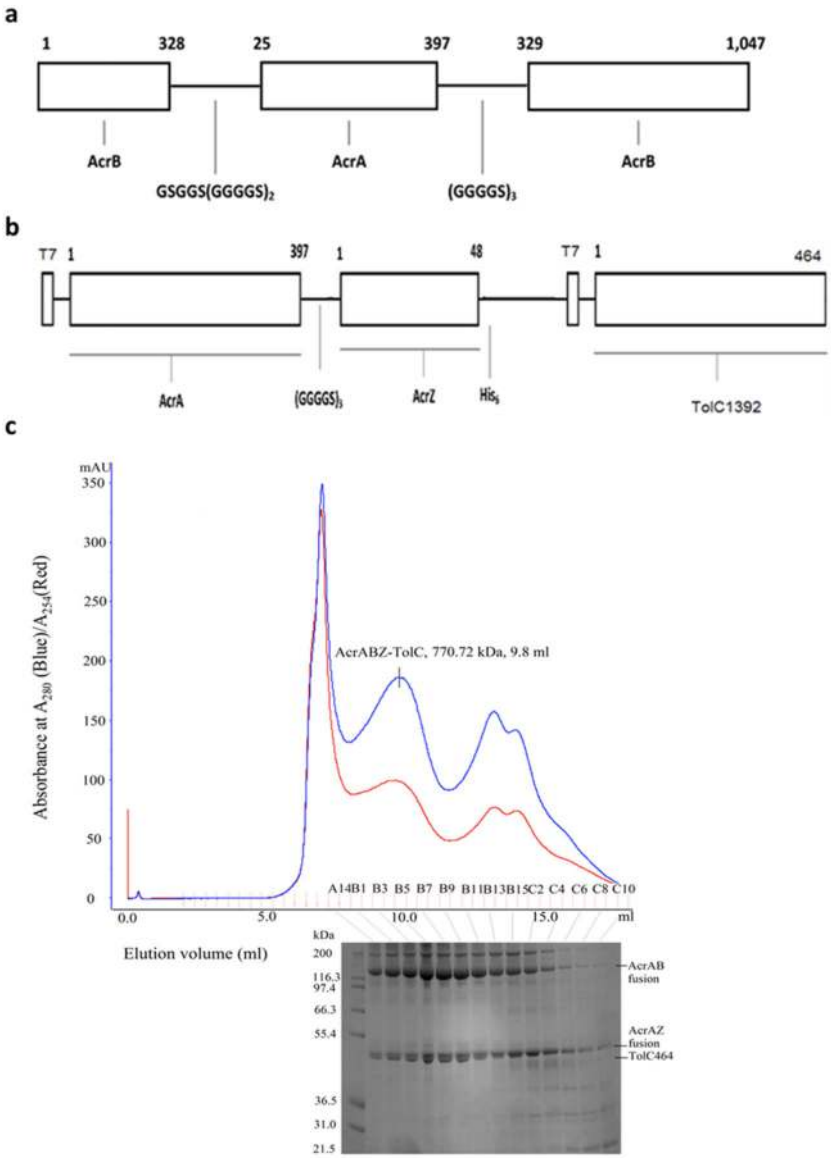

Extended Data Figure 4.

Schematic representations and purification of the fusion proteins used to assemble the efflux pump. (A) The AcrA-AcrB fusion, with two flexible poly(Gly-Ser) linkers. Two C-terminal histidines of AcrB have been removed to prevent binding to the NTA matrix during co-purification. (B) The AcrA-AcrZ-His_5 fusion and TolC coexpression construct. The numbers above the bars correspond to the residues of the protein, and due to the restriction site used for cloning, a single glycine residue was inserted after the start codon in both AcrA and AcrZ. The flexible poly(Gly-Ser) linker permits the protomers to manoeuvre. The figure is related to Figure 2 in the main text. (C) Co-purification of TolC with the AcrABZ complexes. SDS-PAGE of the eluate from gel filtration following nickel affinity and size exclusion chromatography purification. The figure is related to Figure 2 in the main text.

Europe PMC Funders Author Manuscripts

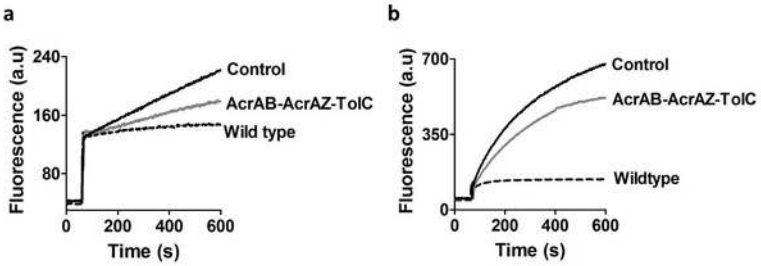

c

Proteins expressed	MIC μg/ml				
	ET	ERY	NOV	HOE	R6G
AcrAZ-fusion + TolC (Negative control: no AcrB)	16	8	16	8	8
AcrAZ-fusion + TolC + AcrB	256	256	256	16	64
AcrAZ-fusion + TolC + AcrAB-fusion	64	16	32	16	32
AcrA-AcrB-TolC (Positive control)	>256	512	1024	>128	>512

ET: Ethidium bromide; ERY: Erythromycin; NOV: Novobiocin; HOE: Hoechst 33342; R6G: Rhodamine 6G. n=4.

Extended data Figure 5.

The fusion assemblies can drive efflux *in vivo*. Drug-transport assays of the AcrAB and AcrAZ fusion proteins in MCΔ*tolC*Δ*acrAB* strain show that the engineered pump has partial activity for efflux of ethidium bromide (A) and trimethylammonium-diphenylhexatriene (B). The results show representative traces from six biological replicates. For ethidium bromide, initial influx rates of 10.3±0.6, 6.4±0.6 and 3.6±0.4 a.u. (arbitrary units)/min were obtained for the non-expressing control cells, the AcrAB-fusion/AcrAZ-fusion/TolC expressing cells and the wild type AcrAB-TolC expressing cells respectively. For trimethylammonium-diphenylhexatriene, initial influx rates of 187±6, 151±3 and 54±2 a.u. (arbitrary units)/min were obtained for the non-expressing control cells, the AcrAB-fusion/AcrAZ-fusion/TolC expressing cells and the wild-type AcrAB-TolC expressing cells respectively. (C) MIC (Minimum inhibitory concentration) data on antimicrobial susceptibility of *Escherichia coli* MCΔ*tolC*Δ*acrAB* cells expressing wild-type AcrA-AcrB-TolC or the fusion proteins with TolC. These data indicate that the fusion of AcrA-AcrZ and the insertion of AcrA into AcrB both diminish the capacity for drug resistance. The plasmids pET21a, pET21a-AcrB or pET21a-$acrB_{328}$-*polyGS*-*acrA*-*polyGS*-$acrB_{329}$ (AcrAB) together with plasmid pRSFduet-1-*acrA*-*polyGS*-$acrZ_{His5}$-*tolC* (AcrAZ + TolC) were transformed into MCΔ*tolC*Δ*acrAB*. Cells were tested for their ability to resist increasing concentrations of cytotoxic drugs. As a positive control, cells were transformed with plasmid pBAD_AcrA+AcrB+TolC, which encodes for the native AcrA-AcrB-TolC efflux pump.

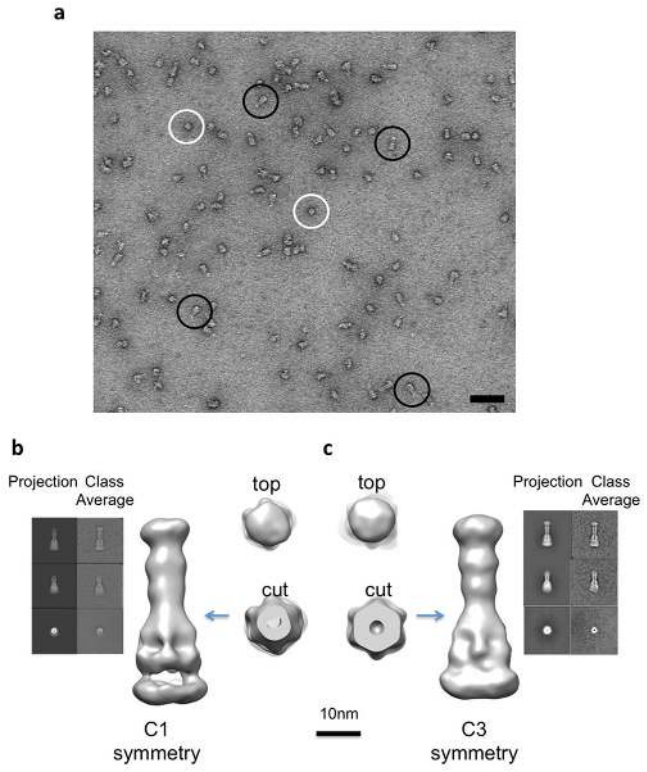

Extended data Figure 6.

Electron microscopy images and class averages of the AcrABZ-TolC complex. (A) Negative stain EM images of the purified AcrABZ-TolC complex after GraFix treatment. White circles indicate particles with long axis aligned close to the normal to the plane of view; black circles show particles with the long axis parallel to the viewing plane. (B) and (C) Class averages from cryo-EM data and reconstructions with C1 symmetry and with C3 symmetry respectively. The galleries in the side panels show representative two-dimensional class averages of the purified pump. The upper panel shows views perpendicular to the long axis of the drumstick shape, the middle panel shows inclined views, and the lower panel shows views along the long axis. The reconstructed images and cross sections indicate the presence of a six-fold symmetry, which is consistent with 6 AcrA protomers. The pseudo-atomic model has three protomers of AcrB and TolC, and as TolC and AcrB each have an internal structural repeat, they have pseudo six-fold symmetry at low resolution (cut view). Both maps are consistent with each other. This figure is related to Figure 2 in the main text.

Europe PMC Funders Author Manuscripts

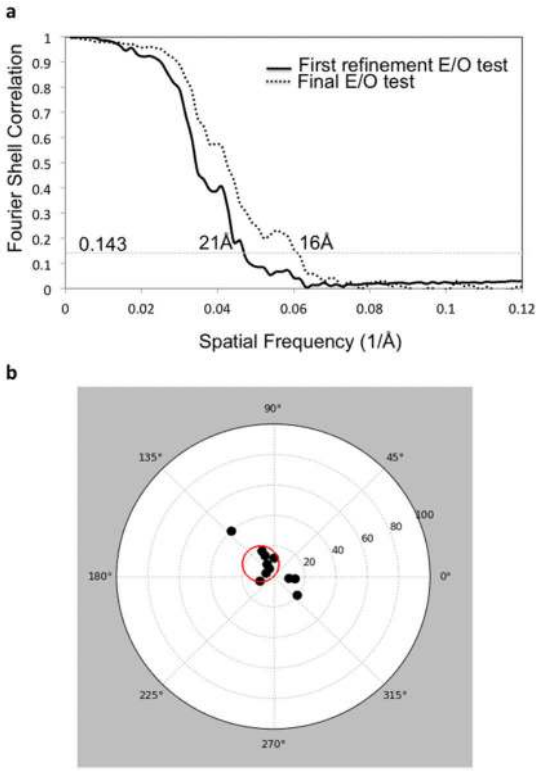

Extended Data Figure 7.

Cryo-EM map resolution estimation and map validation. A) Fourier shell correlation (FSC) of two independently determined cryo-EM maps of the efflux pump assembly after their alignment by Foldhunter[62]. B) Tilt-pair validation of the efflux pump assembly. Each point represents a pair of particles with experimentally known relative tilt. The radius indicates the computationally determined amount of tilt, and the azimuth indicates tilt direction. The red circle denotes particle pairs that cluster around the experimental tilt axis geometry thus validating the map in Figure 2.

Europe PMC Funders Author Manuscripts

Europe PMC Funders Author Manuscripts

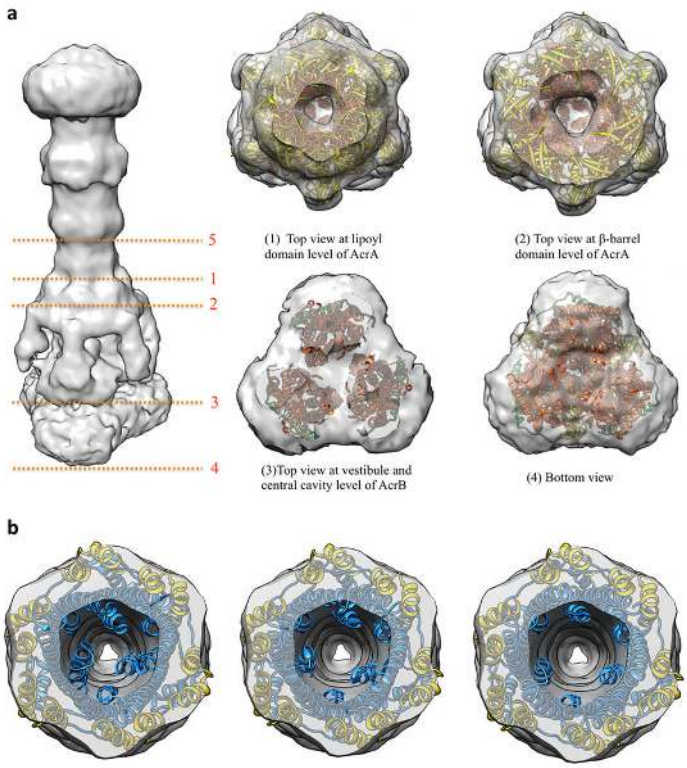

Extended data Figure 8.

Sections through the EM map. A) Slices 1-4: View of planes normal to the three-fold symmetry axis of the pump. B) Slice 5 of pump assembly showing the opening of TolC periplasmic domain. The same transverse plane through the cryo-EM map is shown for with TolC in the closed state, as seen in the crystal structure of the protein in isolation (left, PDB ID: 1EK9), the partially open structure, made by mutations (middle, PDB ID: 2XMN) and the modelled fully opened structure (right).

Extended Data Table 1

Crystallographic data and refinement statistics

Crystal	AcrB/AcrZ/DARPin	AcrB/AcrZ
Space group	R32 (H32)	R32 (H32)
Cell dimensions in hexagonal setting		
a,b,c (Å)	145.01, 145.01, 538.34	146.19, 146.19, 543.00
α,β,γ (°)	90, 90, 120	90, 90, 120
Resolution (Å)	30.0-3.30 (3.46-3.30)*	24.89-3.69 (3.99-3.69)
R_{merge}, %	13.4 (98.6)	12.6 (117.0)
Total number of observations	166,656 (22,416)	244483 (50138)
Unique reflections	33,271 (4368)	23077 (4710)
Completeness, %	99.8 (100.0)	94.5 (94.8)
I/σI (outer shell)	11.0 (1.6)	15.1 (2.1)
<I> half-set correlation	0.998 (0.585)	0.999 (0.791)

Crystal	AcrB/AcrZ/DARPin	AcrB/AcrZ
B values Wilson plot/average in structure, $Å^2$	76.6/87.7	148/117.7
Reflections used in refinement	31,614	21,912
Geometry: Ramachandran favoured, allowed, outliers, %	95.2; 4.6; 0.2	94.9; 4.9; 0.3
Rms deviation from ideal values for bond lengths (Å) and bond angles (°)	0.012, 1.456	0.011, 1.57
Number of non-hydrogen atoms in refinement	9452	7997
Refinement (R/R_{free} 5% reflections in test set), %	28.3/32.4	33.9/36.1

The PDB deposition codes for model and structure factors of AcrB/Acrz/DARPin and AcrB/AcrZ are 4C48 and 4CDI respectively.

*Values in parentheses are for highest-resolution shell

Acknowledgements

This work was supported by the Wellcome Trust and HFSP (B.L.) and partly by an NIH grant (P41GM103832 to W. C.). J.E.V. is supported by a Herschel Smith scholarship. T.O. is the recipient of a Cambridge Trust scholarship, an Adam Glinsman award and a Faculty for the Future Fellowship from the Schlumberger Foundation. We thank Len Packman (PNAC, Biochemistry, Cambridge) for mass-spectrometric analyses and Steven J. Ludtke, Michael F. Schmid, Martin Pos, and Rik van Veen for helpful advice and discussions. We are very grateful to the tireless staff at Diamond Light Source for access to facilities and invaluable help.

References

1. Du D, Venter H, Pos KM, Luisi BF. The Machinery and Mechanism of Multidrug Efflux in Gram-negative Bacteria. Microbial Efflux Pumps: Current Research. 2013 Chapter 3.
2. Koronakis V, Sharff A, Koronakis E, Luisi BF, Hughes C. Crystal structure of the bacterial membrane protein TolC central to multidrug efflux and protein export. Nature. 2000; 405:914–919. [PubMed: 10879525]
3. Murakami S, Nakashima R, Yamashita E, Yamaguchi A. Crystal structure of bacterial multidrug efflux transporter AcrB. Nature. 2002; 419:587–593. [PubMed: 12374972]
4. Mikolosko J, Bobyk K, Zgurskaya HI, Ghosh P. Conformational flexibility in the multidrug efflux system protein AcrA. Structure. 2006; 14:577–587. [PubMed: 16531241]
5. Seeger MA, Schiefner A, Eicher T, Verrey F, Diederichs K, Pos KM. Structural asymmetry of AcrB trimer suggests a peristaltic pump mechanism. Science. 2006; 313:1295–1298. [PubMed: 16946072]
6. Murakami S, Nakashima R, Yamashita E, Matsumoto T, Yamaguchi A. Crystal structures of a multidrug transporter reveal a functionally rotating mechanism. Nature. 2006; 443:173–179. [PubMed: 16915237]
7. Eicher T, Cha H, Seeger MA, Brandstaetter J, El-Delik J, Bohnert JA, Kern WV, Verrey F, Grutter MG, Diederichs K, Pos KM. Transport of drugs by the multidrug transporter AcrB involves an access and a deep binding pocket that are separated by a switch-loop. Proc. Natl. Acad. Sci. U.S.A. 2012; 109:5687–5692. [PubMed: 22451937]
8. Hobbs EC, Yin X, Paul BJ, Astarita JL, Storz G. Conserved small protein associates with the multidrug efflux pump AcrB and differentially affects antibiotic resistance. Proc. Natl. Acad. Sci. U.S.A. 2012; 109:16696–16701. [PubMed: 23010927]
9. Sennhauser G, Amstutz P, Briand C, Storchenegger O, Grütter MG. Drug export pathway of multidrug exporter AcrB revealed by DARPin inhibitors. PLoS Biol. 2007; 5:e7. [PubMed: 17194213]
10. Törnroth-Horsefield S, Gourdon P, Horsefield R, Brive L, Yamamoto N, Mori H, Snijder A, Neutze R. Crystal structure of AcrB in complex with a single transmembrane subunit reveals another twist. Structure. 2007; 15:1663–1673. [PubMed: 18073115]

11. Janganan, et al. Evidence for the assembly of a bacterial tripartite multidrug pump with a stoichiometry of 3:6:3. J. Biol. Chem. 2011; 286:26900–26912. [PubMed: 21610073]
12. Stegmeier JF, Polleichtner G, Brandes N, Hotz C, Andersen C. Importance of the adaptor (membrane fusion) protein hairpin domain for the functionality of multidrug efflux pumps. Biochemistry. 2006; 45:10303–10312. [PubMed: 16922505]
13. Narita, et al. Linkage of the efflux-pump expression level with substrate extrusion rate in the MexAB-OprM efflux pump of *Pseudomonas aeruginosa*. Biochem. Biophys. Res. Commun. 2003; 308:922–926. [PubMed: 12927807]
14. Mima T, Joshi S, Gomez-Escalada M, Schweizer HP. Identification and characterization of TriABC-OpmH, a triclosan efflux pump of Pseudomonasaeruginosa requiring two membrane fusion proteins. J. Bacteriol. 2007; 189:7600–7609. [PubMed: 17720796]
15. Su CC, Long F, Zimmermann MT, Rajashankar KR, Jernigan RL, Yu EW. Crystal structure of the CusBA heavy metal efflux complex of *Escherichia coli*. Nature. 2011; 470:558–562. [PubMed: 21350490]
16. Yum S, Xu Y, Piao S, Sim SH, Kim HM, Jo WS, Kim KJ, Kweon HS, Jeong MH, Jeon H, Lee K, Ha NC. Crystal structure of the periplasmic component of a tripartite macrolide-specific efflux pump. J. Mol. Biol. 2009; 387:1286–1297. [PubMed: 19254725]
17. Kastner B, Fischer N, Golas MM, Sander B, Dube P, Boehringer D, Hartmuth K, Deckert J, Hauer F, Wolf E, et al. GraFix: sample preparation for single-particle electron cryomicroscopy. Nat. Methods. 2008; 5:53–55. [PubMed: 18157137]
18. Tang G, Peng L, Baldwin PR, Mann DS, Jiang W, Rees I, Ludtke SJ. EMAN2: an extensible image processing suite for electron microscopy. J Struct Biol. 2007; 157(1):38–46. [PubMed: 16859925]
19. Scheres SH. RELION: implementation of a Bayesian approach to cryo-EM structure determination. J. Struct. Biol. 2012; 180:519–530. [PubMed: 23000701]
20. Henderson R, Chen S, Chen JZ, Grigorieff N, Passmore LA, Ciccarelli L, Rubinstein JL, Crowther RA, Stewart PL, Rosenthal PB. Tilt-pair analysis of images from a range of different specimens in single-particle electron cryomicroscopy. J Mol Biol. 2011; 413(5):1028–1046. PMCID3220764. [PubMed: 21939668]
21. Berthaud A, Manzi J, Pérez J, Mangenot S. Modeling detergent organization around aquaporin-O using small angle X-ray scattering. J. Am. Chem. Soc. 2012; 134:10080–10088. [PubMed: 22621369]
22. Symmons MF, Bokma E, Koronakis E, Hughes C, Koronakis V. The assembled structure of a complete tripartite bacterial multidrug efflux pump. Proc. Natl. Acad. Sci. U.S.A. 2009; 106:7173–7178. [PubMed: 19342493]
23. Touze T, Eswaran J, Bokma E, Koronakis E, Hughes C, Koronakis V. Interactions underlying assembly of the *Escherichia coli* AcrAB-TolC multidrug efflux system. Mol Microbiol. 2004; 53:697–706. [PubMed: 15228545]
24. Xu Y, Moeller A, Jun S-Y, Le M, Yoon B-Y, Kim J-S, Lee K, Ha N-C. Assembly and channel opening of outer membrane protein in tripartite drug efflux pumps of Gram-negative bacteria. J. Biol. Chem. 2012; 287:11740–11750. [PubMed: 22308040]
25. Trépout S, Taveau J-C, Houssain B, Granier T, Ducruix A, Frangakis AS, Lambert O. Structure of reconstituted bacterial membrane efflux pump by cryo-electron tomography. Biochim. Biophys. Acta. 2010; 1798:1953–1960. [PubMed: 20599691]
26. Tikhonova EB, Yamada Y, Zgurskaya HI. Sequential mechanism of assembly of multidrug efflux pump AcrAB-TolC. Chem Biol. 2011; 18:454–463. [PubMed: 21513882]
27. Ge Q, Yamada Y, Zgurskaya H. The C-terminal domain of AcrA is essential for the assembly and function of the multidrug efflux pump AcrAB-TolC. J. Bacteriol. 2009; 191:4365–4371. [PubMed: 19411330]
28. Janganan TK, Bavro VN, Zhang L, Borges-Walmsley MI, Walmsley AR. Tripartite efflux pumps: energy is required for dissociation, but not assembly or opening of the outer membrane channel of the pump. Mol. Microbiol. 2013; 88:590–602. [PubMed: 23565750]

29. Bavro VN, Pietras Z, Furnham N, Pérez-Cano L, Fernández-Recio J, Pei XY, Misra R, Luisi B. Assembly and channel opening in a bacterial drug efflux machine. Mol Cell. 2008; 30(1):114–21. [PubMed: 18406332]
30. Tikhonova EB, Zgurskaya HI. AcrA, AcrB, and TolC of *Escherichia coli* form a stable intermembrane multidrug efflux complex. J Biol Chem. 2004; 279:32116–32124. [PubMed: 15155734]
31. Miroux B, Walker JE. Over-production of proteins in *Escherichia coli*: mutant hosts that allow synthesis of some membrane proteins and globular proteins at high levels. J. Mol. Biol. 1996; 260:289–298. [PubMed: 8757792]
32. Sennhauser G, Amstutz P, Briand C, Storchenegger O, Grütter MG. Drug export pathway of multidrug exporter AcrB revealed by DARPin inhibitors. PLoS Biol. 2007; 5(1):e7. [PubMed: 17194213]
33. Kabsch W. Automatic processing of rotation diffraction data from crystals of initially unknown symmetry and cell constants. J. Appl. Cryst. 1993; 26:795–200.
34. Evans P. Scaling and assessment of data quality. Acta Crystallogr D Biol Crystallogr. 2006; 62(Pt 1):72–82. [PubMed: 16369096]
35. Eicher T, Cha H, Seeger MA, Brandstaetter J, El-Delik J, Bohnert JA, Kern WV, Verrey F, Grutter MG, Diederichs K, Pos KM. Transport of drugs by the multidrug transporter AcrB involves an access and a deeep binding pocket that are separated by a switch-loop. Proc. Natl. Acad. Sci. U.S.A. 2012; 109:5687–5692. [PubMed: 22451937]
36. Brünger AT, Adams PD, Clore GM, DeLano WL, Gros P, Grosse-Kunstleve RW, Jiang JS, Kuszewski J, Nilges M, Pannu NS, Read RJ, Rice LM, Simonson T, Warren GL. Crystallography & NMR system: A new software suite for macromolecular structure determination. Acta Crystallogr D Biol Crystallogr. 1998; 54:905–921. [PubMed: 9757107]
37. Brunger AT. Version 1.2 of the Crystallography and NMR system. Nat Protoc. 2007; 2(11):2728–33. [PubMed: 18007608]
38. Adams PD, Afonine PV, Bunkoczi G, Chen VB, Davies IW, Echols N, Headd JJ, Hung LW, Kapral GJ, Grosse-Kunstleve RW, McCoy AJ, Moriarty NW, Oeffner R, Read RJ, Richardson DC, Richardson JS, Terwilliger TC, Zwart PH. PHENIX: a comprehensive Python-based system for macromolecular structure solution. Acta Cryst. D Biol Crystallogr. 2010; 66:213–221. [PubMed: 20124702]
39. Murshudov GN, Vagin AA, Lebedev A, Wilson KS, Dodson EJ. Efficient anisotropic refinement of macromolecular structures using FFT. Acta Crystallogr D Biol Crystallogr. 1999; 55(Pt 1):247–55. [PubMed: 10089417]
40. Murshudov GN, Skubák P, Lebedev AA, Pannu NS, Steiner RA, Nicholis RA, Winn MD, Long F, Vagin AA. REFMAC5 for the refinement ofmacromolecular crystal structures. Acta Crystallogr D Biol Crystallogr. 2011; 67:355–367. [PubMed: 21460454]
41. Emsley P, Lohkamp B, Scott W, Cowtan K. Features and development of Coot. Acta Crystallogr D Biol Crystallogr. 2010; 66:486–501. [PubMed: 20383002]
42. Welch A, Awah CU, Jing S, van Veen HW, Venter H. Promiscuous partnering and independent activity of MexB, the multidrug transporter protein from *Pseudomonas aeruginosa*. Biochem J. 2010; 430(2):355–64. [PubMed: 20583998]
43. Lobedanz S, Bokma E, Symmons MF, Koronakis E, Hughes C, Koronakis V. A periplasmic coiled-coil interface underlying TolC recruitment and the assembly of bacterial drug efflux pumps. Proc Natl Acad Sci U S A. 2007; 104(11):4612–7. [PubMed: 17360572]
44. Touzé T, Eswaran J, Bokma E, Koronakis E, Hughes C, Koronakis V. Interactions underlying assembly of the Escherichia coli AcrAB-TolC multidrug efflux system. Mol Microbiol. 2004; 53:697–706. [PubMed: 15228545]
45. Kastner B, Fischer N, Golas MM, Sander B, Dube P, Boehringer D, Hartmuth K, Deckert J, Hauer F, Wolf E, et al. GraFix: sample preparation for single-particle electron cryomicroscopy. Nat. Methods. 2008; 5:53–55. [PubMed: 18157137]
46. Stark H. GraFix: stabilization of fragile macromolecular complexes for single particle cryo-EM. Methods Enzymol. 2010; 481:109–26. [PubMed: 20887855]

47. Tang G, Peng L, Baldwin PR, Mann DS, Jiang W, Rees I, Ludtke SJ. EMAN2: an extensible image processing suite for electron microscopy. J Struct Biol. 2007; 157(1):38–46. [PubMed: 16859925]
48. Li X, Mooney P, Zheng S, Booth CR, Braunfeld MB, Gubbens S, Agard DA, Cheng Y. Electron counting and beam-induced motion correction enable near-atomic-resolution single-particle cryo-EM. Nat Methods. 2013; 10(6):584–90. [PubMed: 23644547]
49. Ludtke SJ, Baldwin PR, Chiu W. EMAN: semiautomated software for high-resolution single-particle reconstructions. J Struct Biol. 1999; 128(1):82–97. [PubMed: 10600563]
50. Scheres SH. RELION: implementation of a Bayesian approach to cryo-EM structure determination. J. Struct. Biol. 2012; 180:519–530. [PubMed: 23000701]
51. Henderson R, Chen S, Chen JZ, Grigorieff N, Passmore LA, Ciccarelli L, Rubinstein JL, Crowther RA, Stewart PL, Rosenthal PB. Tilt-pair analysis of images from a range of different specimens in single-particle electron cryomicroscopy. J Mol Biol. 2011; 413(5):1028–46. [PubMed: 21939668]
52. Murray SC, Flanagan J, Popova OB, Chiu W, Ludtke SJ, Serysheva II. Validation of cryo-EM structure of IP_3R1 channel. Structure. 2013; 21(6):900–9. [PubMed: 23707684]
53. Pettersen EF, Goddard TD, Huang CC, Couch GS, Greenblatt DM, Meng EC, Ferrin TE. UCSF Chimera--a visualization system for exploratory research and analysis. J Comput Chem. 2004; 25(13):1605–12. [PubMed: 15264254]
54. Pei XY, Hinchliffe P, Symmons MF, Koronakis E, Benz R, Hughes C, Koronakis V. Structures of sequential open states in a symmetrical opening transition of the TolC exit duct. Proc Natl Acad Sci U S A. 2011; 108(5):2112–7. [PubMed: 21245342]
55. Koronakis V, Sharff A, Koronakis E, Luisi BF, Hughes C. Crystal structure of the bacterial membrane protein TolC central to multidrug efflux and protein export. Nature. 2000; 405:914–919. [PubMed: 10879525]
56. Mikolosko J, Bobyk K, Zgurskaya HI, Ghosh P. Conformational flexibility in the multidrug efflux system protein AcrA. Structure. 2006; 14:577–587. [PubMed: 16531241]
57. Symmons MF, Bokma E, Koronakis E, Hughes C, Koronakis V. The assembled structure of a complete tripartite bacterial multidrug efflux pump. Proc. Natl. Acad. Sci. U.S.A. 2009; 106:7173–7178. [PubMed: 19342493]
58. Tsukazaki T, Mori H, Echizen Y, Ishitani R, Fukai S, Tanaka T, Perederina A, Vassylyev DG, Kohno T, Maturana AD, Ito K, Nureki O. Structure and function of a membrane component SecDF that enhances protein export. Nature. 2011; 474(7350):235–8. [PubMed: 21562494]
59. Hsieh YH, Zhang H, Wang H, Yang H, Jiang C, Sui SF, Tai PC. Reconstitution of functionally efficient SecA-dependent protein-conducting channels: transformation of low-affinity SecA-liposome channels to high-affinity SecA-SecYEG-SecDF·YajC channels. Biochem Biophys Res Commun. 2013; 431(3):388–92. [PubMed: 23337498]
60. du Plessis DJ, Nouwen N, Driessen AJ. The Sec translocase. Biochim Biophys Acta. 2011; 1808(3):851–65. [PubMed: 20801097]
61. Ashkenazy H, Erez E, Martz E, Pupko T, Ben-Tal N. ConSurf 2010: calculating evolutionary conservation in sequence and structure of proteins and nucleic acids. Nucleic Acids Res. 2010; 38:W529–W533. [PubMed: 20478830]
62. Jiang W, Baker ML, et al. Bridging the information gap: computational tools for intermediate resolution structure interpretation. J Mol Biol. 2001; 308(5):1033–1044. [PubMed: 11352589]

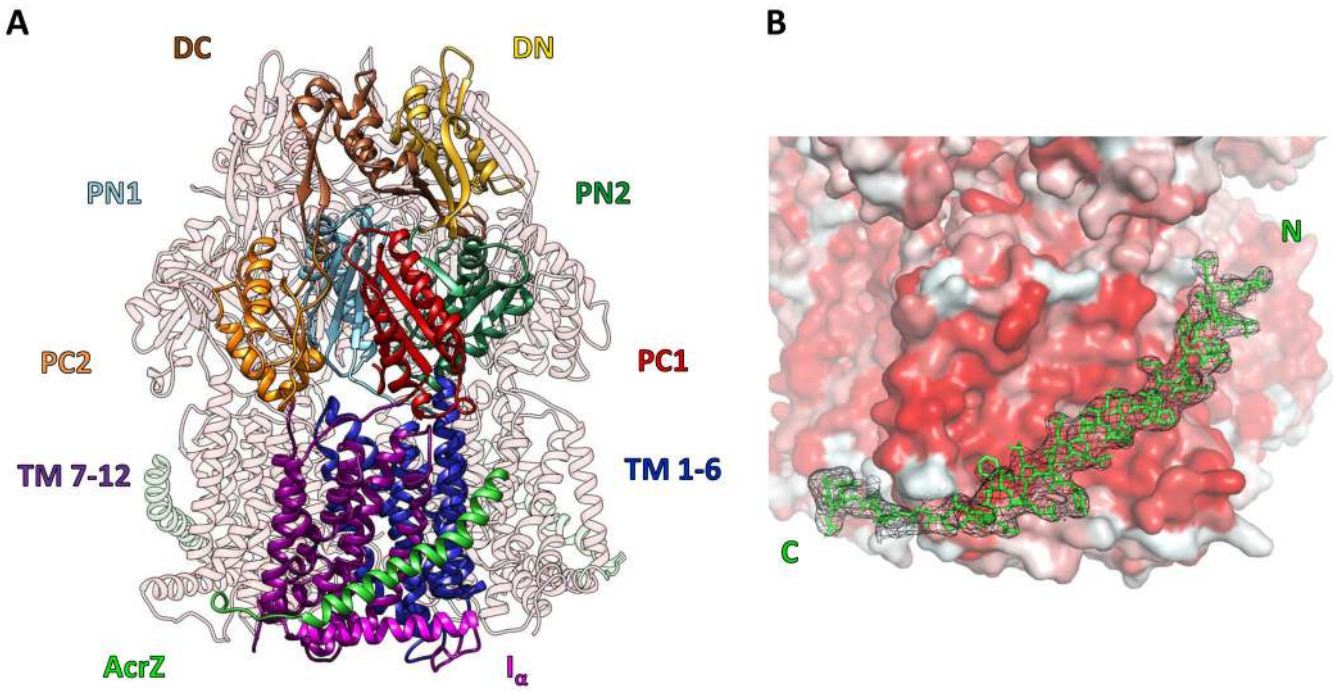

Figure 1.

The crystal structure of the inner-membrane protein AcrB in complex with AcrZ. A) Overall view of the AcrB/AcrZ trimer. The subdomains of an AcrB protomer are labelled: PN1, PN2, PC1, PC2, DN and DC; the transmembrane helices are labelled TM1-6, TM7-12 and the linking helix is labelled Iα. AcrB contains a structural repeat and the structural units comprise PN1-PN2-DN-TM1-6 and PC1-PC2-DC-TM7-12. The protein was crystallized with a DARPin, and one is engaged to the AcrB protomer in the crystallographic asymmetric unit (not shown for clarity). B) Electron density map with coefficients 2Fo-Fc overlaid on the model for AcrZ (green sticks), the contour level is 1 σ. AcrB is shown in surface representation, with residues coloured according to their relative hydrophobicity (hydrophobic in red, hydrophilic in white).

Europe PMC Funders Author Manuscripts

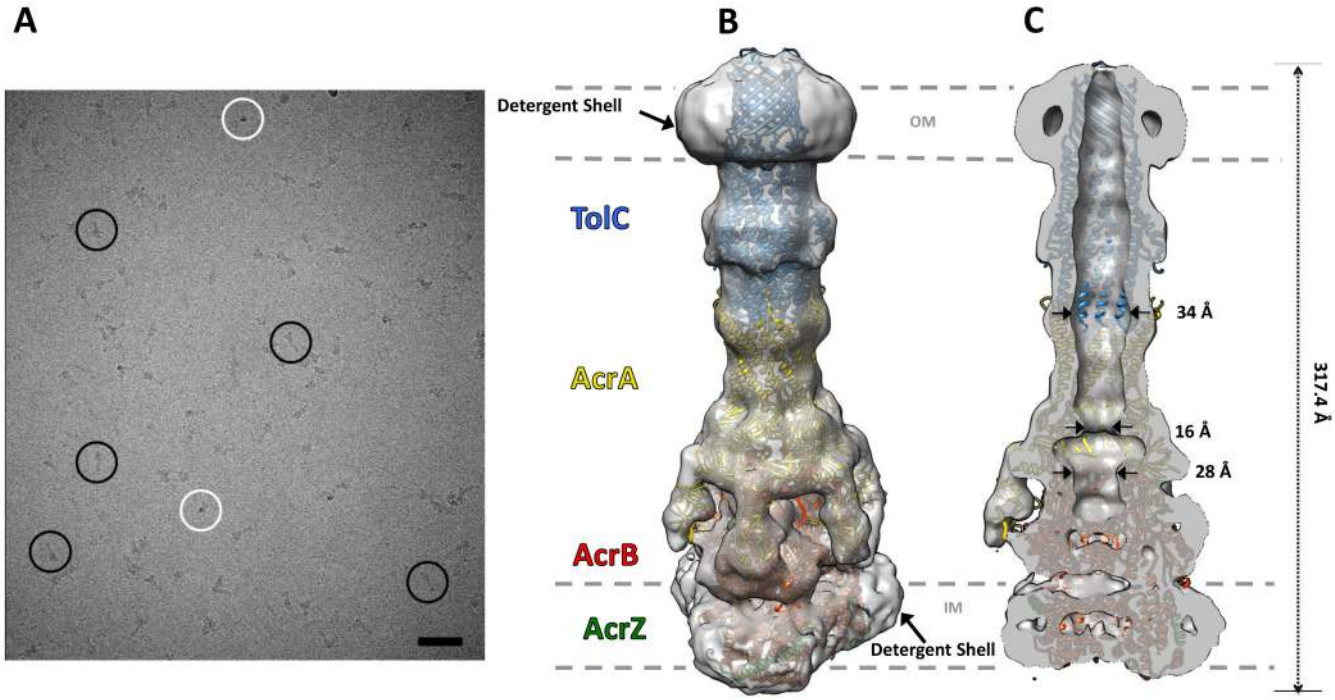

Figure 2.

Cryo-EM image and a pseudoatomic model of the drug efflux pump. A) A representative raw image of the purified pump. White circles indicate particles with long axis aligned close to the normal to the plane of view; black circles show particles with the long axis parallel to the viewing plane. The scale bar shows 50 nm. B) The reconstructed map and pseudoatomic model. TolC and AcrBZ are homotrimers that engage six protomers of AcrA to form an assembly with a protein mass of 771 kDa. AcrA has a composite structure of four linearly discontinuous domains connected with flexible linkers[4] (see also Figure 3A). C) A slice through the reconstruction and model, which shows the continuous conduit that runs from the AcrB funnel through the TolC porin domain.

Europe PMC Funders Author Manuscripts

Europe PMC Funders Author Manuscripts

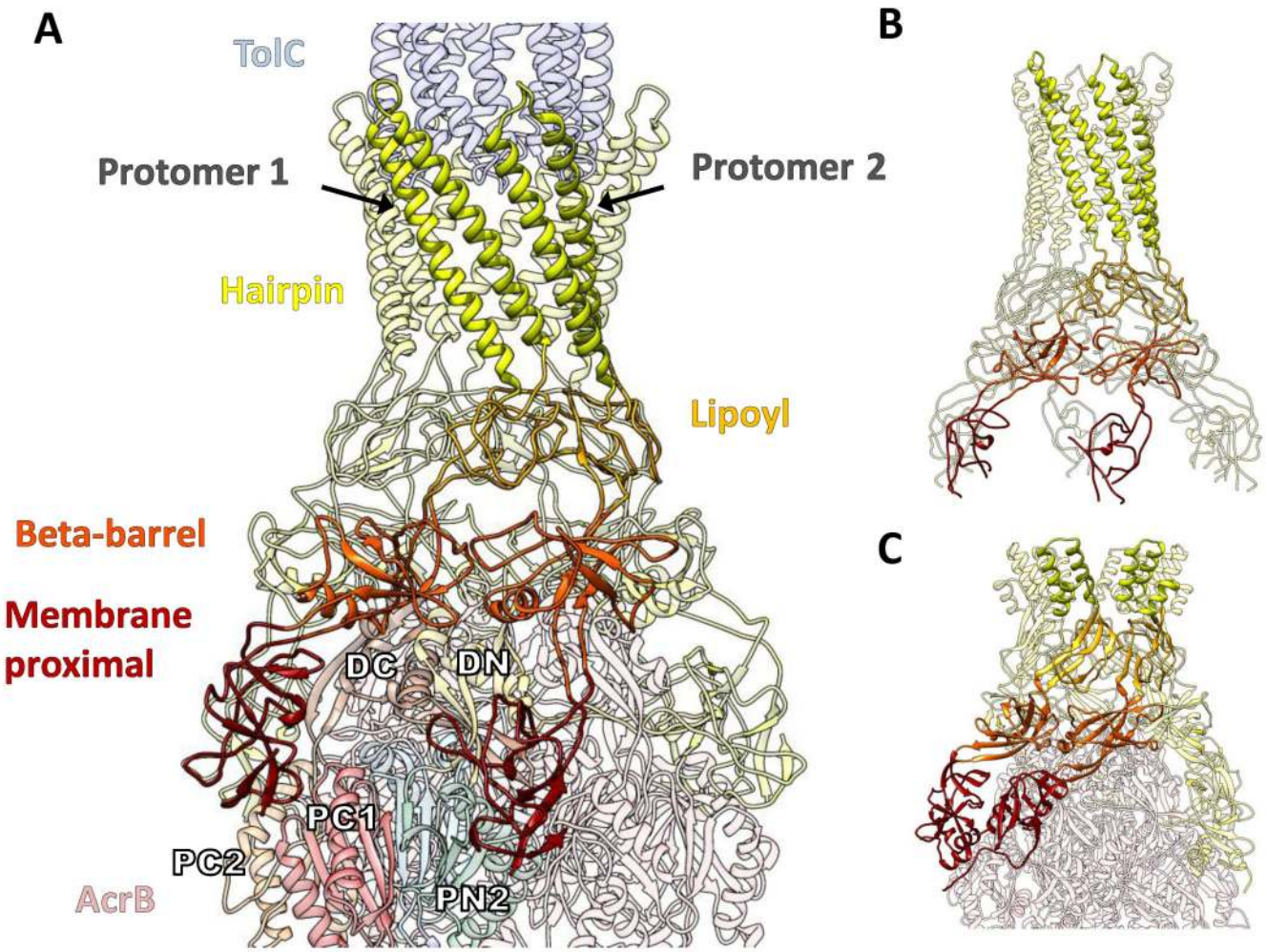

Figure 3.

Modelled interactions of the efflux pump components. A) Interactions of the AcrA hairpin domain with TolC and the AcrA β-barrel and membrane-proximal domains with AcrB. The lipoyl domains principally interact with each other and make no interactions with AcrB or TolC. Two AcrA protomers in the hexameric ring are shown to illustrate the domain-domain interactions. B) Homohexameric subunit organization in the structure of the AcrA homologue, *Actinobacillus actinomycetemcomitans* MacA (PDB ID: 4DK0). C) Interactions of *E. coli* CusA with CusB from the metal-efflux pump[15].